March 15, 2005 / Vol. 30, No. 6 / OPTICS LETTERS 673

Effect of spherical aberration and surface waves on propagation of lens-coupled terahertz pulses

M. T. Reiten and R. A. Cheville

School of Electrical and Computer Engineering, Oklahoma State University, 202 Engineering South, Stillwater, Oklahoma 74078

Received November 23, 2004

Spatiotemporal measurements of a near-single-cycle terahertz pulse emitted from a photoconductive switch terahertz (THz) source show the effects of spherical aberration and surface waves on the pulse shape. The measured phase front has a swallow-tail shape described by catastrophe theory that contributes to the concentric ring structure of THz beam profiles. A time-of-flight model shows that the pulse shape is due to propagation along a cusp caustic and enhancement of the wings of the swallow-tail pulse is caused by surface waves. © 2005 Optical Society of America

OCIS codes: 320.5550, 080.1010, 260.3090.

Ultrashort pulses reshape even in dispersion-free, linear media when approaching the single-cycle limit and originating from optical elements that change the phase front of the pulse. For example, very short optical pulses undergo reshaping near the focus of a lens because of spherical aberration.[1] An experimentally tractable way to measure single-cycle pulse propagation is through generation and detection of terahertz (THz) pulses[2] and mapping of the electric field with high spatial and temporal resolution.[3] Several authors have investigated THz pulse reshaping in diffraction,[4] Gaussian mode coupling efficiency,[5] and time reversal imaging.[6]

Here we show that the inverse analog of pulse reshaping at the focus of a lens[1] affects the spatiotemporal phase front of lens-coupled optically generated THz pulses. A THz pulse outcoupled from a collimating lens exhibits a universal swallowtail shape[7] described by catastrophe theory. This shape results from both spherical aberration and surface waves[2] and contributes to the observed concentric-ring structure of near-field THz beams.[3,5,8]

The experimental setup used has been discussed previously[3] and is shown schematically in Fig. 1(a). The optically generated THz pulse is polarized along $\hat{\mathbf{x}}$ and propagates along $\hat{\mathbf{z}}$. The silicon collimating lens [Fig. 1(b)] has a 5-mm radius of curvature and a 6.45-mm total height[5] and is cemented to the dipole substrate to eliminate beam clipping from mounting hardware. The frequency-independent radiation pattern of the THz dipole source is shown in the left half of Fig. 1(b) for S and P polarizations. Raster scans (80 points, 160-μm spacing) using a fiber-coupled dipole antenna[3] spatially mapped the THz field along the y (S polarization) and x (P polarization) axes at distances of 16 and 3.2 mm from the surface of the silicon lens, respectively.

The measured pulse shape at 16 mm [Fig. 2(a)] is a planar pulse front followed by trailing edges or wings classified in catastrophe theory as a swallowtail cusp.[7] Measurements of the time-resolved field at $y=0$, 2, and 4 mm are overlaid on the figure. The spatial amplitude distribution at five discrete frequencies, obtained from a numerical Fourier transform, is shown in Fig. 2(b). The frequency-dependent spatial amplitude distribution results from interference between the time-delayed wings of the swallowtail and the leading edge. Figure 2(c) shows the pulse structure at 3.2 mm (20λ at 1.9 THz) from the source lens. Spatial inhomogeneities of the source field arise both from the field pattern of a dipole on a surface[9] [Fig. 1(b)] and because the critical angle in silicon is near Brewster's angle, leading to more-efficient coupling around the annulus of the lens.[3] The increased field amplitude in an annular region close to the lens is indicated by arrows in Fig. 2(c). The broad trailing edge

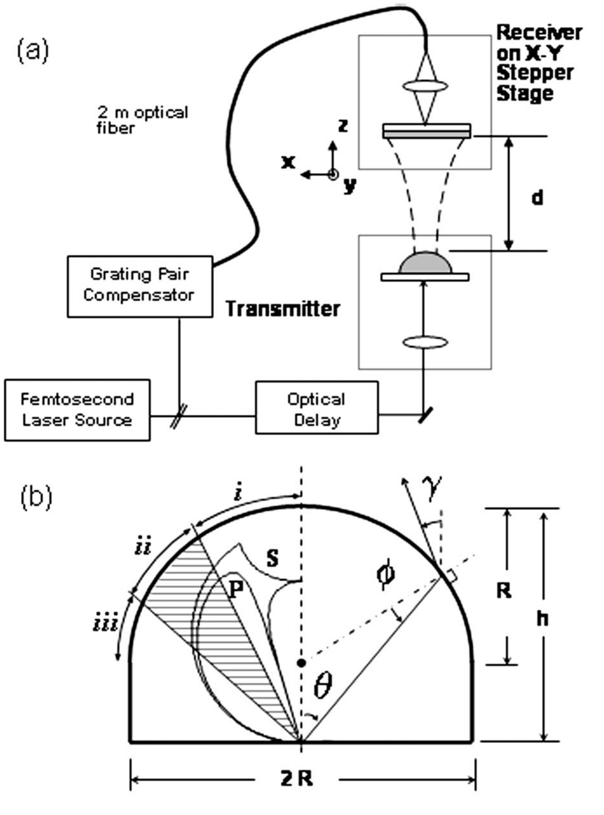

Fig. 1. (a) Spatiotemporal THz measurement system. (b) Collimating silicon lens illustrating regions i, ii, and iii, the field patterns for S and P polarization, and angles θ, γ, and ϕ.

0146-9592/05/060673-3/$15.00 © 2005 Optical Society of America

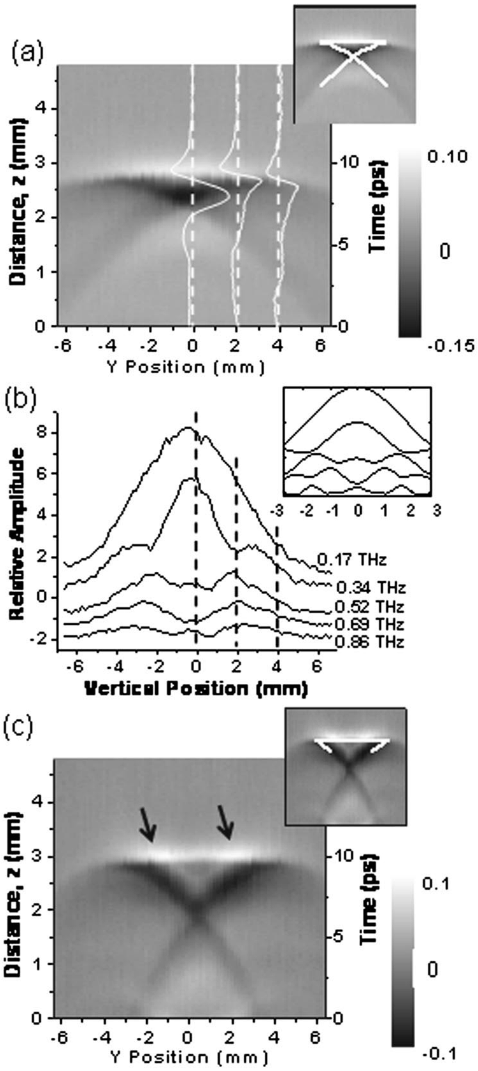

Fig. 2. (a) THz electric field at 16 mm with overlay of measured pulses at $y = 0$, 2, and 4 mm. Solid line in inset is time-of-flight model prediction. (b) Spatial amplitude distribution of the field at five discrete frequencies. The inset is the calculated field distribution. (c) THz field at 3.2 mm; arrows show annular field distribution near the surface of the lens. Inset shows the time-of-flight model predictions of pulse structure.

of the pulse in Fig. 2(c) is due to efficient coupling of low-frequency components to free space owing to surface waves.

To describe the swallowtail pulse shape in the near-field region of the lens, three regions—direct (*i*), marginal (*ii*), and surface waves (*iii*)—are illustrated in Fig. 1(b). These regions are determined by angles θ, γ, and ϕ defined in Fig. 1(b). In the direct region (*i*), $\gamma < 0$ and rays never cross the optical axis, originating from a 6.00-mm-diameter aperture. The marginal region (*ii*) emits rays that cross the axis of propagation ($\gamma > 0$) but are incident on the lens under the critical angle. The marginal region is between the direct ray region and a 9.15-mm-diameter aperture, contributing heavily to the pulse because of the dipole field pattern and large values of the Fresnel transmission coefficients. The surface ray region (*iii*) is where ϕ is beyond the critical angle. The field external to the lens is typically evanescent, but energy may be coupled to free space through surface waves owing to the curved geometry of the interface.[10]

The stationary-phase approximation, $\delta\Phi/\delta\Psi = 0$, is used to determine the time of flight of the pulse front.[11] Φ is the accumulated phase for a given frequency component, $\Phi = k_o\Psi$, to any spatial point (y, z), determined from angle-dependent optical path length Ψ:

$$\Psi = n_L(R^2 + w^2 + 2Rw\cos\beta)^{1/2} + [(R\sin\beta - z)^2 + (y + R - R\cos\beta)^2]^{1/2}, \qquad (1)$$

where $\beta = \phi + \gamma$, $w = h - R$, and $n_L = 3.42$ is the index of refraction of the silicon lens. Although most rigorous in the high-frequency limit, time-of-flight models can be valid for near-single-cycle pulses.[2] For a swallowtail pulse the phase function contains three stationary points (pulses).

The evolution of the pulse front calculated from the time-of-flight model is shown as a heavy solid line in Fig. 3(a) at 90, 133, and 300 ps after optical excitation; the lighter dashed lines represent normals to the phase front (rays).[7] In the far field the stationary points of the leading and trailing edges of the swallowtail approach the same limit, a spherical phase front. The insets in Figs. 2(a) and 2(c) show a comparison of the time-of-flight analysis (white line) with the measured pulses. The flat leading edge of the swallowtail pulse corresponds to the contribution by

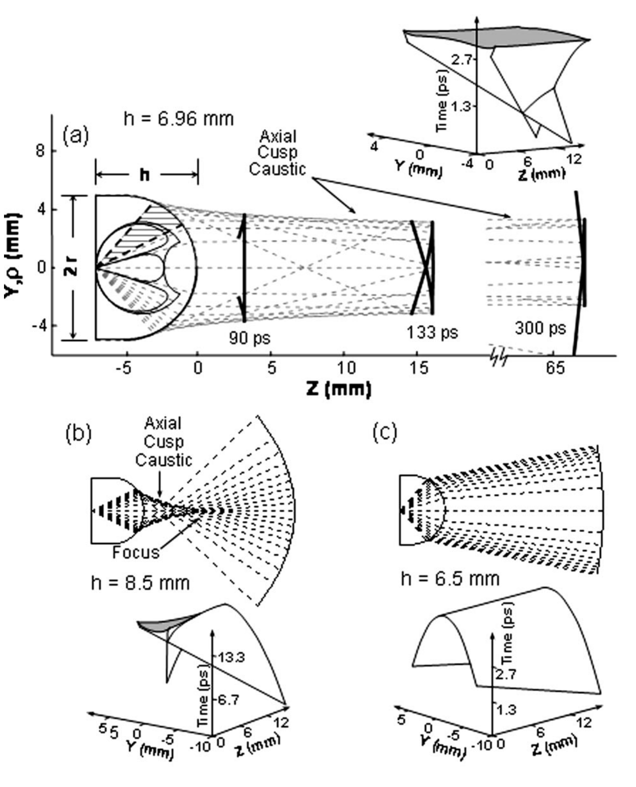

Fig. 3. (a) Stationary phase analysis of the collimating lens system. The inset is the pulse front surface corresponding to this lens. The ray diagrams (above) and pulse front surfaces for focusing and aplanatic hyperhemispherical lenses are shown in (b) and (c), respectively.

direct rays (*i*), whereas the trailing edges of the swallowtail pulse are from marginal and surface rays (*ii, iii*). The inset in Fig. 2(b) shows the spatially resolved amplitude distribution from the time-of-flight model with the trailing edge pulse amplitude of 40% of the leading edge and a near-π phase shift owing to propagation through a caustic.[11] The calculated interference is multiplied by a Gaussian distribution with a 4.5-mm waist. The simple model qualitatively reproduces the amplitude distribution observed, with the exception that the calculated distributions have smaller spatial extent, possibly because of diffraction.

The time-of-flight model does not account for surface waves generated in region iii of the lens as seen by disagreement of the time-of-flight model [inset in Fig. 2(c)] with the observed pulse shapes at $d = 3.2$ mm. The time-of-flight model (white line) predicts that the geometric shadow of the lens surface will obscure the trailing wings of the pulse front coupled out of region ii. The trailing wings of the swallowtail pulse arise from radiation of surface waves[12] generated by the pulse front incident on the lens surface in region iii. The critical angle is strictly defined in the limit of r/λ approaching ∞, i.e., for flat surfaces. For THz frequencies (λ at 0.5 THz $= 600\ \mu$m) and the 5-mm lens curvature, coupling into surface waves becomes wavelength dependent,[12] creating a caustic tangent to the lens surface.[10]

The origin of the swallowtail pulse front is thus due to both surface waves and the effect of the lens on the pulse front. A lens in the paraxial limit produces a planar phase front from a diverging spherical wave by introducing a phase delay proportional to the square of the transverse position (ρ^2). However, outside the paraxial limit the pulse front exhibits phase shifts caused by third-order (Seidel) aberrations.[11] Since the source dipole lies on the optical axis, only spherical aberration contributes, introducing a quartic (ρ^4) phase delay.

Catastrophe theory[13,14] classifies the behavior of families of polynomial equations, i.e., spherical aberration, according to the number of solutions at each point in a parameter space, here the number of stationary phase points at each location in space–time. Rays in Fig. 3(a) represent spatial solutions on which stationary values of the phase delay occur at some undetermined time. A caustic surface is the boundary between regions of space at which the number of real solutions changes. As shown in Fig. 3(a), three rays intersect at any point within the caustic; i.e., there are three phase extrema. The temporal locations of these extrema are the pulse fronts of the swallowtail pulse; the leading edges are local minima, whereas the trailing edges are local maxima. At the caustic boundary the solutions are degenerate and overlap.[13]

Catastrophe theory classifies caustics resulting from a quartic phase correction (ρ^4) as A_3, or axial cusp caustics.[14] Since the phase delay for any ray intersecting a caustic surface at a given point is constant, the shape of the caustic determines the pulse front at any given time[7] and a caustic of a given codimension will generate a pulse front described by the catastrophe of the next-highest codimension.[7,15] Thus an A_3 spatial caustic (ρ^4 phase delay) will have a pulse front of the form of A_4 (fifth-order polynomial) in time,[7,15,16] which corresponds to the observed swallowtail pulse. The A_4 pulse front maps out a surface in space–time that represents the stationary points of the phase [inset in Fig. 3(a)], demonstrating the evolution of the THz pulse as a function of y, z, and time. The A_3 cusp caustic, or projection on the $\hat{\mathbf{y}}\hat{\mathbf{z}}$ plane, is shaded.

The temporal shape of the THz pulse coupled to free space, is dependent on the lens geometry. Lenses with a large h focus the THz pulse, and beyond the focus the pulse front becomes nearly spherical as shown in Fig. 3(b). Figure 3(c) illustrates the phase front for small h, the aplanatic hyperhemispheric lens[5] that exhibits no real caustics, only single solutions to the ray propagation outside the lens. Although the collimating lens [Fig. 3(a)] has a focus at infinity with three real solutions for all Z, the three solutions approach the same limiting value at large distances and a spherical phase front is experimentally observed.[3]

The authors acknowledge the support of the National Science Foundation (NSF9984896), the Army Research Office (40992-PH-DPS), and the Department of Energy (DE-FG02-02ER45960). R. A. Cheville's e-mail address is kridnix@okstate.edu.

References

1. Z. Bor, Opt. Lett. **14**, 119 (1989).
2. D. M. Mittleman, ed., *Sensing with Terahertz Radiation* (Springer-Verlag, Berlin, 2003).
3. M. T. Reiten, S. A. Harmon, and R. A. Cheville, J. Opt. Soc. Am. B **20**, 2215 (2003).
4. S. Hunsche, S. Feng, H. G. Winful, A. Leitenstorfer, M. C. Nuss, and E. P. Ippen, J. Opt. Soc. Am. A **16**, 2025 (1999).
5. J. Van Rudd and D. M. Mittleman, J. Opt. Soc. Am. B **19**, 319 (2002).
6. A. B. Ruffin, J. Decker, L. Sanchez-Palencia, L. Le Hors, J. F. Whitaker, T. B. Norris, and J. V. Rudd, Opt. Lett. **26**, 681 (2001).
7. P. L. Marston, in *Physical Acoustics* (Academic, New York, 1992), pp. 2–221.
8. P. U. Jepsen and S. R. Keiding, Opt. Lett. **20**, 807 (1995).
9. W. Lukosz and R. E. Kunz, J. Opt. Soc. Am. **67**, 1607 (1977).
10. L. Felsen, J. Opt. Soc. Am. **66**, 751 (1976).
11. M. Born and E. Wolf, *Principles of Optics*, 7th ed. (Cambridge U. Press, New York, 1999).
12. J. A. Lock, J. Opt. Soc. Am. A **18**, 3085 (2001).
13. V. I. Arnold, *Catastrophe Theory*, 3rd ed. (Springer-Verlag, Berlin, 1992).
14. T. Poston and I. N. Stewart, *Catastrophe Theory and Its Applications* (Pitman, London, 1978).
15. G. Dangelmyer and W. Guttinger, Geophys. J. R. Astron. Soc. **71**, 79 (1982).
16. M. G. Brown, J. Acoust. Soc. Am. **79**, 1367 (1986).